

Spin-state engineering of single titanium adsorbates on ultrathin magnesium oxide

Received: 31 July 2025

Accepted: 4 January 2026

Soo-hyon Phark, Hong Thi Bui, We-hyo Seo, Yaowu Liu, Valeria Sheina, Curie Lee, Christoph Wolf, Andreas J. Heinrich, Roberto Robles & Nicolás Lorente

Cite this article as: Phark, S.-h., Bui, H.T., Seo, W.-h. *et al.* Spin-state engineering of single titanium adsorbates on ultrathin magnesium oxide. *Nat Commun* (2026). <https://doi.org/10.1038/s41467-026-68314-6>

We are providing an unedited version of this manuscript to give early access to its findings. Before final publication, the manuscript will undergo further editing. Please note there may be errors present which affect the content, and all legal disclaimers apply.

If this paper is publishing under a Transparent Peer Review model then Peer Review reports will publish with the final article.

Spin-State Engineering of Single Titanium Adsorbates on Ultrathin Magnesium Oxide

Soo-hyon Phark^a,^{1,2} Hong Thi Bui,^{1,3} We-hyo Seo,^{1,2} Yaowu Liu,^{1,2} Valeria Sheina,^{1,2} Curie Lee,^{1,3} Christoph Wolf^a,^{1,2} Andreas J. Heinrich,^{1,3} Roberto Robles,⁴ and Nicolás Lorente^a^{4,5}

¹*Center for Quantum Nanoscience,*

Institute for Basic Science (IBS), Seoul 03760, Republic of Korea

²*Ewha Womans University, Seoul 03760, Republic of Korea*

³*Department of Physics, Ewha Womans University, Seoul 03760, Republic of Korea*

⁴*Centro de Física de Materiales CFM/MPC (CSIC-UPV/EHU),*

20018 Donostia-San Sebastián, Spain

⁵*Donostia International Physics Center (DIPC),*

20018 Donostia-San Sebastián, Spain

Abstract

Single atomic adsorbates on ultrathin insulating films provide a promising route towards building bottom-up quantum architectures based on atomically identical yet individually addressable spin qubits on solid surfaces. A key challenge in engineering quantum-coherent spin nanostructures lies in understanding and controlling the spin state of individual adsorbates. In this work, we investigate single titanium (Ti) atoms adsorbed on MgO/Ag(100) surfaces using a combined scanning tunneling microscopy and electron spin resonance. Our measurements reveal two distinct spin states, $S = 1/2$ and $S = 1$, depending on the local adsorption site and the thickness of the MgO film. Density functional theory calculations suggest a Ti^+ configuration for the Ti adsorbates with approximately 3 electrons in the $4s$ and $3d$ valence shells. Using multi-orbital magnetic multiplet calculations the site dependence of the spin can be rationalized as a charge redistribution between spin-polarizing and depolarizing orbitals. These findings underscore the potential of surface-supported single atoms as spin qubits with tunable spin and charge states, enabling atom-by-atom control in the realization of a versatile quantum platform on surfaces.

^aCorresponding authors:

phark@qns.science, wolf.christoph@qns.science and nicolas.lorente@ehu.eus

INTRODUCTION

Positioning individual atoms using the tip of a scanning tunneling microscope (STM) has paved the way for the bottom-up fabrication of tailored nanostructures on surfaces with atomic precision.[1] Subsequent achievements have highlighted the potential of single atoms on surfaces as basic building blocks for constructing nanoscale devices with diverse charge and spin functionalities, exploiting the atomic precision of STM.[2, 3] By choosing an appropriate substrate, it is possible to tune the properties of atomic spins,[4–6] particularly given the subatomic scale of magnetic phenomena.[7]

The implementation of electron spin resonance (ESR) in STM experiments has pushed the spectroscopic energy resolution to an extraordinary limit of ~ 10 neV, and has enabled the coherent manipulation of individual spin states since the first unequivocal continuous-wave ESR spectra were obtained from iron (Fe) single adsorbates on two-monolayer (2 ML) magnesium oxide (MgO) films grown on a silver substrate.[8–11]

Atoms or molecules hosting an electronic spin $S = 1/2$, when coupled to a magnetic field, serve as natural two-level systems and are promising candidates for building solid-surface quantum platforms composed of identical but individually addressable qubits.[12–14] ESR-STM studies on a variety of $S = 1/2$ systems, including titanium (Ti),[15] iron(II) phthalocyanine (FePc),[16, 17] alkali dimers and pairs on MgO,[18] molecular radicals,[19, 20] and bis(phthalocyaninato)terbium(III) on sodium chloride (NaCl),[21] have demonstrated the suitability of single-spin adsorbates for quantum-coherent experiments at the atomic scale. In particular, Ti atoms on MgO have enabled the realization of advanced ESR control protocols, including universal single-qubit gates, a two-qubit gate,[13, 22] and the observation of the free coherent evolution of entangled spins.[23]

Despite these advances, the practical implementation of atomic spin qubits in quantum technologies remains challenging. This is largely due to the complex interplay between adsorbates and substrates, which can induce deviations from free-atom configurations—both in charge and spin states—and may result in reduced coherence times. A detailed understanding of the physical and chemical environment of single atoms on surfaces is therefore essential for the controlled realization of scalable quantum-coherent nanostructures.

The charge and spin states of individual adsorbates can differ substantially from their isolated counterparts, due to mechanisms such as charge transfer, ligand-field effects, or

chemical reactions during deposition. For instance, Ti atoms expected to have $S = 1$ in the gas phase have been reported to exhibit $S = 1/2$ on MgO/Ag(100), an observation previously attributed to hydrogen capture from residual gas.[15, 24–26] Similarly, FePc has been observed to change its spin state from $S = 1$ to $S = 1/2$ due to electron transfer from the Ag substrate.[16, 17] A systematic understanding of how the substrate modifies the electronic configuration of adsorbates is thus a prerequisite for designing robust atomic-scale quantum systems.

The first studies of Ti adsorbates on MgO/Ag(100) concluded that Ti could not explain the experimental evidence showing a spin-1/2 system and proposed the formation of a TiH species.[15] These conclusions were based on density-functional-theory (DFT) calculations in which Ti adatoms were modeled on free-standing MgO layers, without including the metallic Ag(100) substrate present in the experiments. The calculations yielded a spin $S = 1/2$ for adsorbed TiH and $S = 1$ for bare Ti, independent of the adsorption site. Consequently, later studies of Ti on MgO/Ag(100) adopted the assumption of TiH formation to explain their experimental data.[15, 25, 26] In the present work, we show that DFT descriptions of Ti adsorbates are highly sensitive to the delicate balance between charge transfer and electronic correlations. Despite the shortcomings of DFT, our calculations show that Ti can have $S=1/2$ and $S=1$ when adsorbed on MgO/Ag (100) depending on the adsorption site and MgO thickness.

In this work, we combine scanning tunneling spectroscopy (STS), ESR, DFT, and magnetic multiplet calculations to investigate the spin and charge states of Ti atoms adsorbed on MgO films of two and three monolayers (MgO⁽²⁾ and MgO⁽³⁾) grown on Ag(100). We find that the spin state of the adsorbate depends sensitively on both the local adsorption geometry and the MgO thickness. Specifically, Ti exhibits a spin $S = 1/2$ when adsorbed on both oxygen-atop (O-atop) and O–O bridge sites of MgO⁽²⁾, and on bridge sites of MgO⁽³⁾. In contrast, on O-atop sites of MgO⁽³⁾ we find a spin $S > 1/2$, identified via remote-spin ESR, STS, and multiplet calculations. Atom manipulation confirms robust and reversible switching between these distinct spin states and adsorption geometries. Our DFT calculations support a consistent Ti⁺ oxidation state primarily governed by the lowering of the work function by the MgO layer. The Ti spin can be rationalized as a charge redistribution between spin-polarizing and depolarizing orbitals that we model by $4s^23d^1$ and $4s^13d^2$ configurations in our magnetic multiplet calculations. These findings indicate that the interaction with the

adsorption site, rather than chemical doping or hydrogenation, is the principal mechanism for spin variability, providing new avenues for the quantum engineering of surface-supported spin qubits.

RESULTS

A. Experiment

1. *STM images and STS spectra*

The sample was prepared by depositing Ti and Fe atoms with a submonolayer coverage (< 1%) onto defect-free MgO films grown on a clean Ag(100) substrate (see Methods and Supplementary Section 1). Figure 1A presents an STM topography of the sample surface, which includes regions of MgO⁽²⁾, MgO⁽³⁾, and bare Ag. Well-isolated atomic adsorbates are observed throughout all regions.

High-resolution STM images on MgO⁽²⁾ (Fig. 1B) reveal two distinct Ti adsorption geometries: one atop surface oxygen atoms (Ti_O⁽²⁾), and one bridging two adjacent oxygen atoms (Ti_B⁽²⁾), consistent with earlier reports [27, 28]. Similarly, on MgO⁽³⁾ (Fig. 1C), two Ti species are also identified. The bridge-site configuration (Ti_B⁽³⁾) appears with considerable abundance and shows STS characteristics closely resembling those of Ti_B⁽²⁾. In contrast, the oxygen-atop configuration (Ti_O⁽³⁾) displays a much larger apparent height in STM images and distinct spectroscopic features (Fig. 1E), which are discussed in detail below. A third, minor O-atop variant, similar to Ti_O⁽²⁾, was also occasionally observed on MgO⁽³⁾ but accounted for less than 0.1% of the total Ti adsorbate population. This minority species is not considered further (see Fig. S2).

To probe the electronic properties of the four dominant Ti configurations identified in STM (Figs. 1B and C), we performed STS measurements (Figs. 1D and E). The spectra acquired for Ti adsorbates on MgO⁽²⁾ exhibit features in agreement with previous studies [15, 23, 29]. Likewise, Ti_B⁽³⁾ exhibits a nearly identical spectral profile to Ti_B⁽²⁾, characterized by a smooth, monotonic conductance curve and a step-like feature at zero bias (marked by a cyan triangle), attributed to spin polarization of the STM tip [28, 30]. In contrast, Ti_O⁽³⁾ exhibits a pronounced inelastic tunneling (IET) signature at ± 18 meV (orange arrows in the inset), symmetrically positioned about $V_b = 0$. This feature indicates a zero-field splitting

and the presence of a sizable magnetic anisotropy energy (MAE),[31] consistent with a spin state $S > 1/2$. DFT and multiplet calculations for $\text{Ti}_\text{O}^{(3)}$ confirm that this state corresponds to a magnetic ground state with spin $S = 1$ (see the theory section below).

2. ESR spectra

ESR measurements of the Ti adsorbates provided direct insight into their spin states (Fig. 2A). Three species— $\text{Ti}_\text{O}^{(2)}$, $\text{Ti}_\text{B}^{(2)}$, and $\text{Ti}_\text{B}^{(3)}$ —exhibit ESR resonances (red, blue, and cyan traces, respectively) within the frequency range expected for Zeeman splitting under an applied magnetic field of ~ 0.6 T and an effective g -factor of ~ 2 , consistent with a spin angular momentum of $S = 1/2$ [15, 28]. The assignment of $S = 1/2$ for $\text{Ti}_\text{B}^{(3)}$ is further supported by the close resemblance between its dI/dV spectrum (Fig. 1D, blue) and that of $\text{Ti}_\text{B}^{(2)}$ (Fig. 1E, cyan).

In contrast, $\text{Ti}_\text{O}^{(3)}$ does not display any ESR resonance within the same frequency window (orange trace in Fig. 2A), indicating a fundamentally different spin configuration. Coupled with the IET-like steps observed in its dI/dV spectrum at ± 18 meV (Fig. 1E), this suggests a spin state with $S > 1/2$ and significant magnetic anisotropy, warranting further investigation.

To probe the magnetic anisotropy of $\text{Ti}_\text{O}^{(3)}$, we analyzed its interaction with a neighboring spin. In this approach, the target spin ($\text{Ti}_\text{O}^{(3)}$) couples to a nearby probe spin with $S = 1/2$ ($\text{Ti}_\text{B}^{(3)}$), and the anisotropy of the target is inferred from angular variations in the ESR spectrum of the probe [32, 33]. The $\text{Ti}_\text{B}^{(3)}$ – $\text{Ti}_\text{O}^{(3)}$ pair was assembled by lateral manipulation using the STM tip ('dragging'; see Fig. 3C), with a separation of 0.72 nm as denoted in Fig. 2B.

The ESR spectrum acquired on the $\text{Ti}_\text{B}^{(3)}$ in this pair (Fig. 2C) exhibits a clear peak splitting Δf arising from spin–spin interaction, modeled as $J\mathbf{S}_\text{B} \cdot \mathbf{S}_\text{O}$. The angular dependence of Δf with respect to the orientation of the external magnetic field θ_ext (Fig. 3D) follows a $\cos \theta_\text{ext}$ trend [32], consistent with uniaxial out-of-plane anisotropy of the $\text{Ti}_\text{O}^{(3)}$ spin. Given that the $\text{Ti}_\text{B}^{(3)}$ spin aligns with the external field direction, the sinusoidal modulation of $\Delta f(\theta_\text{ext})$ provides strong evidence for a spin angular momentum $S_\text{O} > 1/2$ in $\text{Ti}_\text{O}^{(3)}$. The observation of two sinusoidal branches further suggests bistability in the spin orientation of $\text{Ti}_\text{O}^{(3)}$, with preferred alignment along two collinear directions, which in turn defines the pair

of resonance frequencies observed in the ESR spectrum (see up and down arrows in Fig. 3C).

3. Control of adsorption sites

When adsorbed on $\text{MgO}^{(2)}$, Ti atoms exhibit relatively short spin lifetimes and coherence times, most likely limited by substrate-induced spin scattering in the absence of tunneling electrons. [34] Consequently, Ti atoms adsorbed on thicker insulating layers such as $\text{MgO}^{(3)}$ may exhibit significantly enhanced coherence, owing to the reduced electronic coupling to the underlying Ag substrate, which suppresses backscattering of free electrons [34]. In this context, achieving precise control over Ti atom positioning on $\text{MgO}^{(3)}$ is essential for constructing artificial spin structures with optimized quantum coherence. To this end, we employ two complementary atom manipulation techniques to reposition Ti atoms on $\text{MgO}^{(3)}$, as illustrated in Fig. 3 (see Supplementary Section 2 for technical details).

The first method consists of picking up a $\text{Ti}_\text{O}^{(3)}$ atom with the STM tip and dropping it off at a new location, as shown schematically in Fig. 3A. This approach is suitable for long-distance repositioning, typically resulting in a $\text{Ti}_\text{O}^{(3)}$ species within a $\text{MgO}^{(3)}$ domain. Interestingly, when the atom is dropped onto a $\text{MgO}^{(2)}$ region, the resulting species are either $\text{Ti}_\text{O}^{(2)}$ or $\text{Ti}_\text{B}^{(2)}$, as confirmed by both STM contrast and STS features (see Fig. 3B for $\text{Ti}_\text{O}^{(2)}$). Given the well-established $S = 1/2$ character of Ti adsorbates on $\text{MgO}^{(2)}$ using ESR,[15, 28, 29] this observation, together with the absence of ESR signal (Fig. 2A), supports that a Ti atom adsorbs with different spin-dependent electronic structures depending on the thickness of the MgO layer.

The second method enables short-distance repositioning by inducing lateral hopping of the Ti atom between neighboring lattice sites using voltage pulses applied to the STM junction, as depicted in Fig. 3C ('dragging'). By fine-tuning the lateral tip displacement x_{hop} , vertical approach z_{hop} , and pulse amplitude V_{hop} , we achieve controlled atomic movement over half the O–O lattice spacing on the MgO surface (see sequential STM images in Fig. 3D). This manipulation protocol enables precise construction of multi-atom assemblies, including the $\text{Ti}_\text{B}^{(3)}\text{–}\text{Ti}_\text{O}^{(3)}$ pair discussed in Fig. 2B. Notably, the hopping process is reversible, allowing the Ti atom to switch between two distinct adsorption sites. As demonstrated in Figs. 1E and 2A, this transition induces a corresponding change in the atom's spin, which is either $S > 1/2$ or $S = 1/2$, depending on whether the atom occupies an O-atop or bridge site.

This strongly suggests that the spin state of Ti is governed by its local bonding environment and can be reversibly switched via site-selective manipulation.

B. Theory

In order to rationalize the experimental findings concerning the spin state of adsorbed Ti, we have studied its electronic structure in different environments, including the presence of H. In general, H-adsorption has been suggested to occur in experimental conditions under ultra-high vacuum and low temperatures for Ti adsorbates. [15] Indeed, our DFT calculations show that Ti can readily form stable hydride species when adsorbed on the MgO/Ag(100) surface, see the Supplementary Section 3. Among the considered configurations, TiH_2 emerges as the thermodynamically favored species under hydrogen-rich conditions, as determined by comparing Gibbs free energies referenced to gas-phase H_2 . The formation of TiH_3 is found to be unstable, typically leading to spontaneous H desorption.

TiH has a reduced thermodynamic phase space and can only be formed for a small range of hydrogen chemical potentials. Under low concentration of hydrogen, bare Ti will be stabilized depending on the source of hydrogen that fixes the hydrogen chemical potential. This is further supported by the experimental observation that Ti adatoms can slowly degrade over time and sporadically become spectroscopically dark no longer exhibiting any ESR features. We tentatively assign this latter behavior to a degradation process related to slow hydrogen adsorption that happens on the scale of months, hopefully to be confirmed by a more systematic study.

Under ultra-low temperature and ultrahigh vacuum experimental conditions, Ti atoms are likely found on the surface. A comparison of the theoretically obtained magnetic structures of the TiH_x species indicates that the bare Ti adsorbate is compatible with the experimental data, while TiH does not reproduce the observed behavior (see the Supplementary Section 3, for details).

Our calculations give us access to the adsorption energies, which can be tentatively compared to the relative abundance of adsorbate on the atop and bridge sites. In our experiments, the prevalence of the bridge site on two monolayers is changed to the atop site on three monolayers. This behavior is only reproduced by the chemisorption energy of the Ti adsorbate (Supplementary Section 3).

In the following, we analyze in detail the electronic structure of Ti atoms on $\text{MgO}^{(2)}$ and $\text{MgO}^{(3)}$.

1. *Ti on $\text{MgO}/\text{Ag}(100)$: Electronic Configuration*

Our DFT calculations reveal distinct behavior depending on the adsorption site of Ti (O-atop vs. O-bridge), whereas the influence of MgO thickness ($\text{MgO}^{(2)}$ vs. $\text{MgO}^{(3)}$) is comparatively minor. Based on the experimental evidence, the most probable surface species is a single Ti atom in a positively charged Ti^+ configuration, resulting from charge transfer to the substrate, facilitated by the reduced work function due to the MgO overlayer.

In all cases, charge analysis indicates that Ti adsorbed on $\text{MgO}/\text{Ag}(100)$ retains approximately three valence electrons (see Table 1). While the non-integer values arise from the intrinsic ambiguity in decomposing the DFT total charge density into orbital contributions, the net charge consistently supports a Ti^+ oxidation state.

	Total Charge	3d (up; down)	4s (up; down)	M_{Ti} (μ_{B})
$\text{Ti}_{\text{B}}^{(2)}$	3.02	2.31 (1.51; 0.80)	0.71 (0.28; 0.43)	0.87
$\text{Ti}_{\text{O}}^{(2)}$	3.25	2.42 (2.24; 0.18)	0.82 (0.53; 0.29)	2.31
$\text{Ti}_{\text{B}}^{(3)}$	3.04	2.31 (1.89; 0.42)	0.72 (0.25; 0.47)	1.25
$\text{Ti}_{\text{O}}^{(3)}$	3.16	2.45 (2.24; 0.21)	0.71 (0.49; 0.22)	2.32

TABLE 1: Electronic structure of Ti on $\text{MgO}/\text{Ag}(100)$: The table reports the total ($s+d$) valence charge, the spin-resolved occupations of the $3d$ and $4s$ orbitals, and the total magnetic moment of Ti adsorbed on different MgO sites and thicknesses. While the total occupations remain similar across configurations, the degree of spin polarization (and hence the effective spin state) varies markedly with adsorption site. See text and Supplementary Information for further discussion.

As shown in Table 1, the total $3d$ occupation lies consistently in the range of $d^{2.3}-d^{2.45}$, with the $4s$ orbital slightly less than singly occupied. Despite the similar total electron count, the magnetic moments differ significantly: O-atop configurations yield magnetic moments of $\sim 2.3 \mu_{\text{B}}$, while bridge-site configurations exhibit reduced moments as low as $0.87 \mu_{\text{B}}$ on $\text{MgO}^{(2)}$. This disparity arises not from charge transfer but from spin depolarization within

the occupied states.

Figure 4 displays the projected density of states (PDOS) for Ti adsorbed on MgO/Ag(100). O-atop adsorption (Figs. 4A and B) shows two occupied *d*-orbitals around -1 eV, which yield a magnetic moment close to $2 \mu_B$ (Table 1) for both MgO thicknesses. The *4s* orbital plays only a minor role; instead, two *d*-orbitals in the majority-spin channel are occupied, resulting in an effective spin $S = 1$. This finding aligns well with the experimental results for MgO⁽³⁾, but differs for MgO⁽²⁾, where ESR indicates an $S = 1/2$ configuration.

In bridge-site geometries (Figs. 4C and D), the *d*-orbitals appear at approximately -1 eV below the Fermi level. Depolarizing contributions appear near the Fermi level. These results are consistent with a $d^{2.3}$ configuration of Table 1 with a magnetic moment close to $S = 1/2$.

To further elucidate the observed spin states and particularly the contrasting behavior of Ti on O-atop sites of MgO⁽²⁾ versus MgO⁽³⁾, we performed multiplet calculations assuming three valence electrons in the *s* and *d* shells. In this model, the *4s* orbital acts as a depolarizing channel, mimicking the enhanced hybridization and spin screening expected for bridge-site adsorption. This approach enables us to capture the delicate interplay between orbital configuration and spin state, as explored in the next section.

2. Multiplet calculations

We performed multiplet calculations to understand the DFT results and explore their experimental consequences on STS and ESR data (Figs. 1E and 2A). Following the methodology of Ref. [35], we first determined the relaxed ground-state geometry of the Ti_O⁽³⁾ adsorbate via DFT calculations (Figs. 5A and B). We then generate a local basis set through wannierization, which then serves as input for the multiplet calculation. DFT suggests that the three valence electrons of Ti are in a $3d^24s^1$ configuration. Here, hybridization to the *4s* orbital plays the role of the depolarizing hybridization found in the above DFT calculations, with the *3d* orbitals contain the magnetic properties of the Ti atom. By systematically varying the *4s*-*3d* orbital splitting Δ_{sd} , the multiplet calculations reveal a crossover between the configurations $3d^14s^2$ and $3d^24s^1$ around $\Delta_{sd} \approx 1.2$ eV (Fig. 5C).

Since the DFT electronic structure suggests a $3d^24s^1$ configuration for both Ti_O⁽²⁾ and Ti_O⁽³⁾ we assume that these systems are near the crossover regime. Most likely DFT does not accurately predict Δ_{sd} for MgO⁽²⁾, due to limitations in capturing the Ti intra-atomic

correlations in the presence of external hybridization and lower symmetry. We find that in all systems that show $S = 1/2$ behavior in the experiment DFT predicts a small $3d$ - $4s$ level split and only in 3 ML O-top ($S > 1/2$) shows a significantly increased level separation (see Fig. S6), responsible for stabilizing the $3d^2$ configuration. Remarkably, a single adjustable parameter— Δ_{sd} —is sufficient to reproduce all experimentally observed spin states on $\text{MgO}^{(2)}$ and $\text{MgO}^{(3)}$ without invoking additional charge transfer or a hydrogen adsorption/desorption mechanisms. In the following we use Δ_{sd} to select either a $3d^1$ or $3d^2$ configuration for $\text{MgO}^{(2)}$ and $\text{MgO}^{(3)}$ for the oxygen atop adsorption site, respectively. We calculate differential conductance spectra and find good agreement between simulations and experiments. In particular, the calculated dI/dV spectrum for the $3d^1$ configuration of $\text{MgO}^{(2)}$ (Fig. 5D) qualitatively reproduces the features observed in Fig. 3B, including the crystal-field-induced excitation from the ground-state doublet, which is known to be sensitive to tip-adsorbate distance. Likewise, for the $3d^2$ configuration on $\text{MgO}^{(3)}$, the simulated spectrum in Fig. 5E aligns with the experimental excitation near 20 mV (cf. Fig. 3B).

Finally, we note that the work functions of $\text{MgO}^{(2)}$ and $\text{MgO}^{(3)}$ are nearly identical [36] (see also Fig. S5), which should enable electron transfer from Ti to the Ag substrate for both cases, stabilizing a Ti^+ state in good agreement with the above DFT results. While previous studies have suggested hydrogenation as a cause of spin reduction, [15] our calculations show that hydrogen adsorption mainly alters the $4s$ -like density of states and does not significantly affect the $3d$ orbitals responsible for the observed spin states.

DISCUSSION

We have combined ESR-STM spectroscopy, atom manipulation, and first-principles theory to investigate the spin and charge states of single titanium atoms adsorbed on ultrathin MgO films on Ag(100). Our experiments reveal that the spin state of Ti is strongly site-dependent: Ti adsorbed on O-atop sites of $\text{MgO}^{(3)}$ exhibits a spin $S = 1$, whereas bridge sites of $\text{MgO}^{(2)}$ and $\text{MgO}^{(3)}$, as well as O-atop sites of $\text{MgO}^{(2)}$, yield $S = 1/2$. Atom-by-atom manipulation demonstrates reversible switching between these spin states, excluding irreversible chemical modifications such as hydrogenation as the underlying mechanism.

Density functional theory and multiplet calculations support a Ti^+ charge state with three valence electrons occupying $3d$ and $4s$ orbitals. The observed spin-state variability is

attributed to a competition between spin-polarizing and depolarizing orbital configurations, tunable by the local adsorption geometry and MgO thickness. Thermodynamic analysis rules out TiH and TiH₃ as stable surface species, indicating that either bare Ti or TiH₂ may exist depending on the availability of hydrogen, though experimental evidence points to bare Ti being dominant under typical conditions.

Our findings establish that Ti on MgO can stably host multiple spin states in a chemically pure configuration, tunable via site-selective adsorption. This opens a pathway toward the deterministic design of atomic-scale spin qubits with engineered anisotropy, coherence, and charge states, paving the way for scalable quantum nanostructures on surfaces.

METHODS

Experimental

The methods employed in the experiments mainly involved the preparation of the sample including cleanliness and Ti deposition. This is a critical stage to have reproducible data. The second important methodology is the actual measurement of ESR on the single atoms used in this work.

Sample preparation

An atomically clean Ag(100) substrate was prepared through repeated cycles of Ar⁺ sputtering and thermal annealing. MgO films were grown on the Ag substrate at 580 K by evaporating Mg in an O₂ atmosphere of 1.1×10^{-6} Torr. Fe and Ti atoms were deposited on the MgO surface at < 100 K, by precooling the sample holder in the STM state of liquid helium temperature. The STM tip was fabricated by mechanically cutting a Pt/Ir wire (0.25 mm diameter), and its apex was spin-polarized by picking up Fe atoms from the MgO surface. The tip's spin polarization was calibrated using the asymmetry of the differential conductance (dI/dV) across the zero bias in STS spectra measured from the Ti adsorbates on the oxygen-atop sites of MgO.

Single-atom ESR experiments

STS and ESR measurements were performed on Ti adsorbates on the surfaces of both two- and three-monolayer-thick MgO layers in an ultrahigh-vacuum (UHV) chamber (base pressure $< 10^{-10}$ mbar) using a ³He-cooled STM (Unisoku, USM1300) at $T = 0.4$ K, equipped with two-axis superconducting magnets and high-frequency transmission cables. The ESR measurements were conducted using a commercial RF signal generator (Agilent E8257D), with the RF signal combined with a DC bias voltage through a bias tee (SigaTek, SB15D2). To read out the spin-polarized current in the ESR of the spins, a commercial current preamplifier (Femto, SPECS) followed by a lock-in amplifier (SR860, Stanford Research) was used. The RF signals were modulated at 95 Hz, with the modulation signal sent to the lock-in amplifier as a reference. The bias voltage V_b refers to the sample voltage while the tip is

grounded. The STM constant-current feedback loop was set to open and low gain during the STS and ESR measurements, respectively.

Theoretical

The methods used for our theoretical analysis involve the calculation of highly correlated electronic structure to account for the atomic structure using the Multiplet method, together with general DFT calculations that take into account the interactions between the different parts of this study involving surfaces and atoms. Finally, an important part of the work has been devoted to rationalizing the energetics behind the presence of H, this has been achieved by Gibbs free energy studies.

Multiplet calculations and Wannier basis construction

The multiplet calculations were performed within a Wannier-function framework following Ref. [35]. The Wannierization was carried out starting from a non-spin-polarized GGA calculation, using the same computational parameters described above. An $11 \times 11 \times 1$ \mathbf{k} -point grid was employed, with projections onto the Ti *s* and *d* manifolds and the O *p* manifold.

The resulting Wannier functions associated with the Ti *3d* orbitals are highly localized, with a quadratic spread of $\Omega^2 \approx 1 \text{ \AA}^2$, whereas the Ti *4s* Wannier function is more spatially extended, with $\Omega^2 \approx 3 \text{ \AA}^2$. The resulting basis set comprises six Ti-derived states (one *4s* and five *3d*) together with projections onto the O *2p* states. This choice allows us to analyze the orbital level alignment and, in particular, the energetic splitting between the Ti *s* and *d* states for different adsorption geometries.

The on-site energies extracted from the Wannier Hamiltonian are shown in Fig. S6 for the four adsorption configurations considered. For the MgO⁽²⁾ atop and bridge configurations, as well as for the MgO⁽³⁾ bridge configuration, the on-site levels exhibit a similar structure characterized by a small *s*-*d* energy splitting. These three configurations are therefore expected to host a single unpaired electron on the Ti atom, consistent with the experimentally observed $S = 1/2$ behavior.

In contrast, for the MgO⁽³⁾ atop configuration the Ti *3d* levels are significantly lowered in

energy, stabilizing a $3d^2$ electronic configuration. This electronic structure naturally leads to a higher-spin ground state, in agreement with the experimentally observed $S > 1/2$ behavior.

Density functional theory calculations

DFT calculations have been performed using the plane-wave codes **Quantum Espresso** [37–39] and **VASP** [40, 41]. In addition to the PBE exchange and correlation functional, the calculations used an empirical Hubbard U correction [42] in order to improve the description of localized $3d$ electrons. The chosen value, $U - J = 2.0$ eV, is in agreement with thorough **VASP** DFT calculations [43]. Van der Waals (VdW) interactions were described by the semi-empirical dispersion-forces correction D3 [44]. The calculations were performed using the projector augmented-wave method (PAW) [45] to treat the electron-atom potential. We used complementary calculations of the same system using **VASP** since it has been shown in literature [46] that the ground state for Ti on MgO/Ag was hard to uniquely identify. Our additional calculations confirm the fundamental ground state properties of Ti on MgO/Ag, however they also show subtle differences with respect to energy splitting of the $4s$ and $3d$ states as well as different polarizations close to the Fermi level. This indicates that there is a dependence on the ground state solution on the pseudopotentials since all other factors (e.g. the dispersion correction) were kept consistent across different codes. For the adsorbed species, we need at least a 3×3 unit cell of oxygen atoms to converge the calculations with respect to cell size in order to reproduce single adsorbates. We have used four layers of Ag(100) that are critical to obtain results closer to the experiment.

Gibbs free energy stability calculations

The relative stability of different hydrogenated adsorbates is assessed using the Gibbs free energy,

$$G = H - TS, \quad (1)$$

where H is the enthalpy and TS the entropic contribution. Under the experimental conditions considered here, the relative prevalence of competing adsorption configurations is determined by their Gibbs free energies [47]. In practice, the evaluation of G is based on

total energies obtained from first-principles calculations, with a key ingredient being the chemical potential of the hydrogen reservoir.

Hydrogen is assumed to be supplied in its molecular form, H_2 , which is energetically favorable at the experimental temperature (~ 0.4 K). The chemical potential per hydrogen atom, μ_H , is therefore defined as one half of the dissociation energy of an isolated H_2 molecule,

$$\mu_H = E[H] = \frac{1}{2}E^{(\text{diss})}[H_2], \quad (2)$$

with the energy reference taken as gas-phase H_2 . Alternative hydrogen sources, denoted H_{new} , are incorporated through their chemical potential relative to atomic hydrogen in the gas phase,

$$\Delta\mu = E[H_{\text{new}}] - E[H]. \quad (3)$$

The incremental chemical potential associated with adding one hydrogen atom to a TiH_x adsorbate is computed as

$$\mu_x = E[TiH_x] - (E[TiH_{x-1}] + E[H]), \quad (4)$$

which corresponds to the binding energy of a hydrogen atom in the TiH_x complex. Here, $E[TiH_x]$ denotes the total energy of TiH_x adsorbed on $MgO/Ag(100)$, and $E[H]$ is the reference energy per hydrogen atom.

Within this framework, the change in Gibbs free energy associated with the adsorption of x hydrogen atoms on Ti is given by

$$\Delta G(\Delta\mu) = x\mu_x - x\Delta\mu. \quad (5)$$

At the experimental temperature (~ 0.4 K), additional free-energy contributions arising from molecular rotations, vibrational entropy, configurational entropy, and vapor-pressure effects are negligible compared to chemical bond energies and are therefore omitted. Consequently, evaluating $\Delta G(\Delta\mu)$ as a function of the hydrogen chemical potential provides a direct criterion for the relative thermodynamic stability of different TiH_x species.

DATA AVAILABILITY

The data used and generated in this study have been deposited in the ZENODO repository [48]. The data are available at <https://doi.org/10.5281/zenodo.17938903>

CODE AVAILABILITY

No custom code was generated for this study.

ACKNOWLEDGMENTS

SP, HTB, WS, YL, CW and AJH acknowledge financial support from the Institute for Basic Science (IBS-R027-D1). RR and NL thank projects PID2021-127917NB-I00 by MCIN/AEI/10.13039/501100011033, IT-1527-22 by the Basque Government, 202260I187 by CSIC, ESiM project 101046364 by the EU, and computational resources by Finisterrae III (CESGA). Views and opinions expressed are however those of the author(s) only and do not necessarily reflect those of the EU. Neither the EU nor the granting authority can be held responsible for them. CW thanks Fernando Delgado and Susanne Baumann for insightful discussions.

AUTHOR CONTRIBUTIONS

SP conceived the experiments. SP, HTB, WS, and YL performed the experiments. NL and RR performed the VASP DFT calculations. CW and CL performed QE DFT and multiplet calculations. All authors discussed the results and prepared the manuscript.

COMPETING INTERESTS

The authors declare no competing interests.

- [1] D. M. Eigler, C. P. Lutz, and W. E. Rudg, An atomic switch realized with the scanning tunnelling microscope, *Nature* **352**, 600 (1991).
- [2] S. Loth, S. Baumann, C. P. Lutz, D. M. Eigler, and A. J. Heinrich, Bistability in atomic-scale antiferromagnets, *Science* **335**, 196 (2012).

[3] D.-J. Choi, R. Robles, S. Yan, J. A. J. Burgess, S. Rolf-Pissarczyk, J.-P. Gauyacq, N. Lorente, M. Ternes, and S. Loth, Building complex kondo impurities by manipulating entangled spin chains, *Nano Letters* **17**, 6203 (2017), pMID: 28872317, <https://doi.org/10.1021/acs.nanolett.7b02882>.

[4] D.-J. Choi, N. Lorente, J. Wiebe, K. von Bergmann, A. F. Otte, and A. J. Heinrich, Colloquium: Atomic spin chains on surfaces, *Reviews of Modern Physics* **91**, 041001 (2019).

[5] C. Mier, J. Hwang, J. Kim, Y. Bae, F. Nabeshima, Y. Imai, A. Maeda, N. Lorente, A. Heinrich, and D.-J. Choi, Atomic manipulation of in-gap states in the β -Bi₂Pd superconductor, *Phys. Rev. B* **104**, 045406 (2021).

[6] S. Trishin, C. Lotze, N. Bogdanoff, F. von Oppen, and K. J. Franke, Moiré tuning of spin excitations: Individual Fe atoms on MoS₂/au(111), *Phys. Rev. Lett.* **127**, 236801 (2021).

[7] R. Turanský, K. Palotás, J. Brndiar, Y. J. Li, Y. Sugawara, and I. , Subatomic-scale resolution with spm: Co adatom on p(2 \times 1)Cu(110):O, *Nanotechnology* **30**, 095703 (2019).

[8] S. Baumann, W. Paul, T. Choi, C. P. Lutz, A. Ardavan, and A. J. Heinrich, Electron paramagnetic resonance of individual atoms on a surface, *Science* **350**, 417 (2015).

[9] F. D. Natterer, K. Yang, W. Paul, P. Willke, T. Choi, T. Greber, A. J. Heinrich, and C. P. Lutz, Reading and writing single-atom magnets, *Nature* **543**, 226 (2017).

[10] T. Choi, W. Paul, S. Rolf-Pissarczyk, A. J. Macdonald, F. D. Natterer, K. Yang, P. Willke, C. P. Lutz, and A. J. Heinrich, Atomic-scale sensing of the magnetic dipolar field from single atoms, *Nature nanotechnology* **12**, 420 (2017).

[11] P. Willke, Y. Bae, K. Yang, J. L. Lado, A. Ferrón, T. Choi, A. Ardavan, J. Fernández-Rossier, A. J. Heinrich, and C. P. Lutz, Hyperfine interaction of individual atoms on a surface, *Science* **362**, 336 (2018), <https://www.science.org/doi/pdf/10.1126/science.aat7047>.

[12] A. J. Heinrich, W. D. Oliver, L. M. K. Vandersypen, A. Ardavan, R. Sessoli, D. Loss, A. B. Jayich, J. Fernandez-Rossier, A. Laucht, and A. Morello, Quantum-coherent nanoscience, *Nature Nanotechnology* **16**, 1318 (2021).

[13] Y. Wang, Y. Chen, H. T. Bui, C. Wolf, M. Haze, C. Mier, J. Kim, D.-J. Choi, C. P. Lutz, Y. Bae, S.-h. Phark, and A. J. Heinrich, An atomic-scale multi-qubit platform, *Science* [10.1126/science.adc5050](https://doi.org/10.1126/science.adc5050) (2023), publisher: American Association for the Advancement of Science.

[14] D.-J. Choi, S.-h. Phark, A. J. Heinrich, and N. Lorente, Electron spin resonance with scanning tunneling microscopy: a tool for an on-surface quantum platform of identical qubits, *Nanoscale Advances* **7**, 4551 (2025).

[15] K. Yang, Y. Bae, W. Paul, F. D. Natterer, P. Willke, J. L. Lado, A. Ferrón, T. Choi, J. Fernández-Rossier, A. J. Heinrich, and C. P. Lutz, Engineering the eigenstates of coupled spin-1/2 atoms on a surface, *Phys. Rev. Lett.* **119**, 227206 (2017).

[16] X. Zhang, C. Wolf, Y. Wang, H. Aubin, T. Bilgeri, P. Willke, A. J. Heinrich, and T. Choi, Electron spin resonance of single iron phthalocyanine molecules and role of their non-localized spins in magnetic interactions, *Nature Chemistry* **14**, 59 (2022), number: 1 Publisher: Nature Publishing Group.

[17] P. Willke, T. Bilgeri, X. Zhang, Y. Wang, C. Wolf, H. Aubin, A. Heinrich, and T. Choi, Coherent spin control of single molecules on a surface, *ACS Nano* **15**, 17959 (2021), pMID: 34767351, <https://doi.org/10.1021/acsnano.1c06394>.

[18] S. Kovarik, R. Robles, R. Schlitz, T. S. Seifert, N. Lorente, P. Gambardella, and S. Stepanow, Electron Paramagnetic Resonance of Alkali Metal Atoms and Dimers on Ultrathin MgO, *Nano Letters* **22**, 4176 (2022), publisher: American Chemical Society.

[19] S. Kovarik and S. Stepanow, Spin torque driven electron paramagnetic resonance of a single spin in a pentacene molecule, *Science* (2024).

[20] G. Czap, C. Wolf, J. Reina-Gálvez, M. H. Sherwood, and C. P. Lutz, Magnetic resonance imaging of single organic radicals with sub-molecular resolution (2025), arXiv:2504.18043 [cond-mat.mes-hall].

[21] R. Kawaguchi, K. Hashimoto, T. Kakudate, K. Katoh, M. Yamashita, and T. Komeda, Spatially resolving electron spin resonance of π -radical in single-molecule magnet, *Nano Letters* **23**, 213 (2023), pMID: 36585948, <https://doi.org/10.1021/acs.nanolett.2c04049>.

[22] Y. Wang, M. Haze, H. T. Bui, W.-h. Soe, H. Aubin, A. Ardavan, A. J. Heinrich, and S.-h. Phark, Universal quantum control of an atomic spin qubit on a surface, *npj Quantum Information* **9**, 48 (2023).

[23] L. M. Veldman, L. Farinacci, R. Rejali, R. Broekhoven, J. Gobeil, D. Coffey, M. Ternes, and A. F. Otte, Free coherent evolution of a coupled atomic spin system initialized by electron scattering, *Science* **372**, 964 (2021), publisher: American Association for the Advancement of Science.

[24] P. Willke, Y. Bae, K. Yang, J. L. Lado, A. Ferrón, T. Choi, A. Ardavan, J. Fernández-Rossier, A. J. Heinrich, and C. P. Lutz, Hyperfine interaction of individual atoms on a surface, *Science* **362**, 336 (2018).

[25] K. Yang, W. Paul, S. H. Phark, P. Willke, Y. Bae, T. Choi, T. Esat, A. Ardavan, A. J. Heinrich, and C. P. Lutz, Coherent spin manipulation of individual atoms on a surface, *Science* **366**, 509 (2019).

[26] M. Steinbrecher, W. M. J. van Weerdenburg, E. F. Walraven, N. P. E. van Mullekom, J. W. Gerritsen, F. D. Natterer, D. I. Badrtdinov, A. N. Rudenko, V. V. Mazurenko, M. I. Katnelson, A. van der Avoird, G. C. Groenenboom, and A. A. Khajetoorians, Quantifying the interplay between fine structure and geometry of an individual molecule on a surface, *Phys. Rev. B* **103**, 155405 (2021).

[27] Y. Bae, K. Yang, P. Willke, T. Choi, A. J. Heinrich, and C. P. Lutz, Enhanced quantum coherence in exchange coupled spins via singlet-triplet transitions, *Science Advances* **4**, eaau4159 (2018).

[28] J. Kim, W.-j. Jang, T. H. Bui, D.-J. Choi, C. Wolf, F. Delgado, Y. Chen, D. Krylov, S. Lee, S. Yoon, C. P. Lutz, A. J. Heinrich, and Y. Bae, Spin resonance amplitude and frequency of a single atom on a surface in a vector magnetic field, *Phys. Rev. B* **104**, 174408 (2021).

[29] T. S. Seifert, S. Kovarik, D. M. Juraschek, N. A. Spaldin, P. Gambardella, and S. Stepanow, Longitudinal and transverse electron paramagnetic resonance in a scanning tunneling microscope, *Science Advances* **6**, 10.1126/sciadv.abc5511 (2020).

[30] J. Hwang, D. Krylov, R. Elbertse, S. Yoon, T. Ahn, J. Oh, L. Fang, W.-j. Jang, F. H. Cho, A. J. Heinrich, and Y. Bae, Development of a scanning tunneling microscope for variable temperature electron spin resonance, *Review of Scientific Instruments* **93**, 093703 (2022).

[31] S. Loth, C. P. Lutz, and A. J. Heinrich, Spin-polarized spin excitation spectroscopy, *New J. Phys.* **12**, 125021 (2010).

[32] S.-h. Phark, H. T. Bui, A. Ferrón, J. Fernández-Rossier, J. Reina-Gálvez, C. Wolf, Y. Wang, K. Yang, A. J. Heinrich, and C. P. Lutz, Electric-Field-Driven Spin Resonance by On-Surface Exchange Coupling to a Single-Atom Magnet, *Advanced Science* **10**, 2302033 (2023), eprint: <https://onlinelibrary.wiley.com/doi/pdf/10.1002/advs.202302033>.

[33] S. Reale, J. Hwang, J. Oh, H. Brune, A. J. Heinrich, F. Donati, and Y. Bae, Electrically driven spin resonance of 4f electrons in a single atom on a surface, *Nature Communications*

15, 5289 (2024).

- [34] W. Paul, K. Yang, S. Baumann, N. Romming, T. Choi, C. P. Lutz, and A. J. Heinrich, Control of the millisecond spin lifetime of an electrically probed atom, *Nature Physics* **13**, 403 (2017).
- [35] C. Wolf, F. Delgado, J. Reina, and N. Lorente, Efficient ab initio multiplet calculations for magnetic adatoms on mgo, *The Journal of Physical Chemistry A* **124**, 2318 (2020), pMID: 32098473.
- [36] T. König, G. H. Simon, H.-P. Rust, and M. Heyde, Work function measurements of thin oxide films on metals—mgo on ag(001), *The Journal of Physical Chemistry C* **113**, 11301 (2009), <https://doi.org/10.1021/jp901226q>.
- [37] P. Giannozzi, O. Andreussi, T. Brumme, O. Bunau, M. B. Nardelli, M. Calandra, R. Car, C. Cavazzoni, D. Ceresoli, M. Cococcioni, N. Colonna, I. Carnimeo, A. D. Corso, S. de Gironcoli, P. Delugas, R. A. D. Jr, A. Ferretti, A. Floris, G. Fratesi, G. Fugallo, R. Gebauer, U. Gerstmann, F. Giustino, T. Gorni, J. Jia, M. Kawamura, H.-Y. Ko, A. Kokalj, E. Küçükbenli, M. Lazzeri, M. Marsili, N. Marzari, F. Mauri, N. L. Nguyen, H.-V. Nguyen, A. O. de-la Roza, L. Paulatto, S. Poncé, D. Rocca, R. Sabatini, B. Santra, M. Schlipf, A. P. Seitsonen, A. Smogunov, I. Timrov, T. Thonhauser, P. Umari, N. Vast, X. Wu, and S. Baroni, Advanced capabilities for materials modelling with quantum espresso, *Journal of Physics: Condensed Matter* **29**, 465901 (2017).
- [38] P. Giannozzi, S. Baroni, N. Bonini, M. Calandra, R. Car, C. Cavazzoni, D. Ceresoli, G. L. Chiarotti, M. Cococcioni, I. Dabo, A. Dal Corso, S. de Gironcoli, S. Fabris, G. Fratesi, R. Gebauer, U. Gerstmann, C. Gougoussis, A. Kokalj, M. Lazzeri, L. Martin-Samos, N. Marzari, F. Mauri, R. Mazzarello, S. Paolini, A. Pasquarello, L. Paulatto, C. Sbraccia, S. Scandolo, G. Sclauzero, A. P. Seitsonen, A. Smogunov, P. Umari, and R. M. Wentzcovitch, Quantum espresso: a modular and open-source software project for quantum simulations of materials, *Journal of Physics: Condensed Matter* **21**, 395502 (19pp) (2009).
- [39] P. Giannozzi, O. Baseggio, P. Bonfà, D. Brunato, R. Car, I. Carnimeo, C. Cavazzoni, S. de Gironcoli, P. Delugas, F. Ferrari Ruffino, A. Ferretti, N. Marzari, I. Timrov, A. Urru, and S. Baroni, Quantum espresso toward the exascale, *The Journal of Chemical Physics* **152**, 154105 (2020), <https://doi.org/10.1063/5.0005082>.
- [40] G. Kresse and J. Furthmüller, Efficient iterative schemes for ab initio total-energy calculations using a plane-wave basis set, *Phys. Rev. B* **54**, 11169 (1996).

- [41] G. Kresse and D. Joubert, From ultrasoft pseudopotentials to the projector augmented-wave method, *Phys. Rev. B* **59**, 1758 (1999).
- [42] S. L. Dudarev, G. A. Botton, S. Y. Savrasov, C. J. Humphreys, and A. P. Sutton, Electron-energy-loss spectra and the structural stability of nickel oxide: An LSDA+U study, *Physical Review B* **57**, 1505 (1998).
- [43] Z. Hu and H. Metiu, Choice of U for DFT+ U Calculations for Titanium Oxides, *The Journal of Physical Chemistry C* **115**, 5841 (2011).
- [44] S. Grimme, J. Antony, S. Ehrlich, and H. Krieg, A consistent and accurate ab initio parametrization of density functional dispersion correction (DFT-D) for the 94 elements H-Pu, *The Journal of Chemical Physics* **132**, 154104 (2010).
- [45] P. E. Blöchl, Projector augmented-wave method, *Phys. Rev. B* **50**, 17953 (1994).
- [46] J. Kim, K. Noh, Y. Chen, F. Donati, A. J. Heinrich, C. Wolf, and Y. Bae, Anisotropic hyperfine interaction of surface-adsorbed single atoms, *Nano Letters* **22**, 9766 (2022), pMID: 36317830, <https://doi.org/10.1021/acs.nanolett.2c02782>.
- [47] K. Reuter and M. Scheffler, Composition, structure, and stability of RuO₂(110) as a function of oxygen pressure, *Phys. Rev. B* **65**, 035406 (2001).
- [48] S.-h. Phark, H. T. Bui, W.-h. Seo, Y. Liu, V. Sheina, C. Lee, C. Wolf, A. J. Heinrich, R. Robles, and N. Lorente, Spin-state engineering of single titanium adsorbates on ultrathin magnesium oxide, 10.5281/zenodo.17938903 (2025).

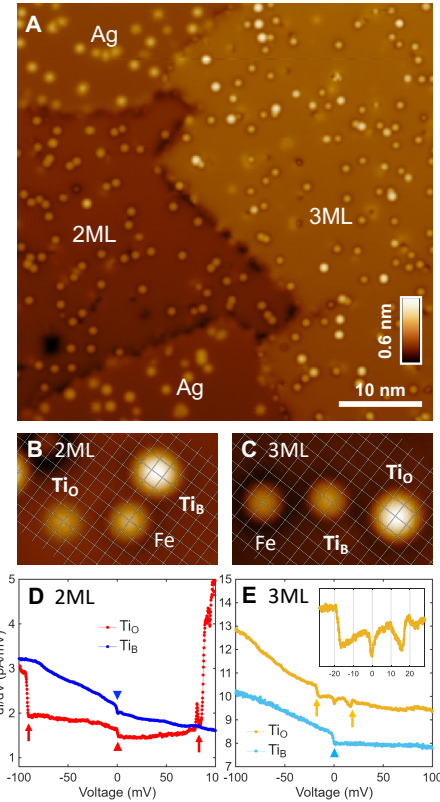


FIG. 1: **Atomic species on MgO/Ag:** (A) An 50×50 nm 2 STM topographic image of the sample surface (B and C) High resolution STM images of 2 ML and 3 ML MgO surfaces with Ti and Fe adsorbates on oxygen-atop sites. Set points: $V_b = 100$ mV and $I_{\text{tun}} = 10$ pA. The overlayed gray meshes indicate the MgO lattice of which each crossing point is the oxygen-atop site. (D and E) STS spectra measured on Ti atoms. Arrows indicate characteristic features stemming from tunneling via inelastic channels. Triangles point the features induced by the spin-polarized tips. The inset in (E) is a zoom-in of the spectrum around zero bias. Set points: $V_b = 100$ mV and $I_{\text{tun}} = 100$ pA.

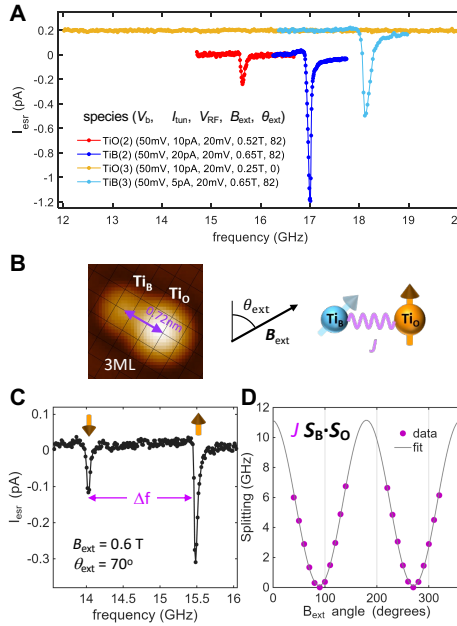


FIG. 2: **ESR of Ti adsorbates on MgO:** (A) ESR spectra measured on the four Ti species. The spectra measured on 3ML are shifted by 0.2 pA for clarity. Measurement conditions for each spectrum are denoted in the legend. (B) STM image of a Ti_B⁽³⁾ with a nearby Ti_O⁽³⁾ at a distance of 0.72 nm, with a depiction of spin-spin coupling (J) and external magnetic field (B_{ext}). The overlayed square mesh indicates the MgO lattice of which each crossing point is the oxygen-atop site. (C) An ESR spectrum measured on the Ti_B⁽³⁾ coupled with a Ti_O⁽³⁾, as shown in B. (D) Field angle dependence of the splitting (Δf) measured from ESR spectra. Gray curve is a fit of Δf to $\cos(\theta_{\text{ext}})$. The angle of the external field (θ_{ext}) is depicted in B.

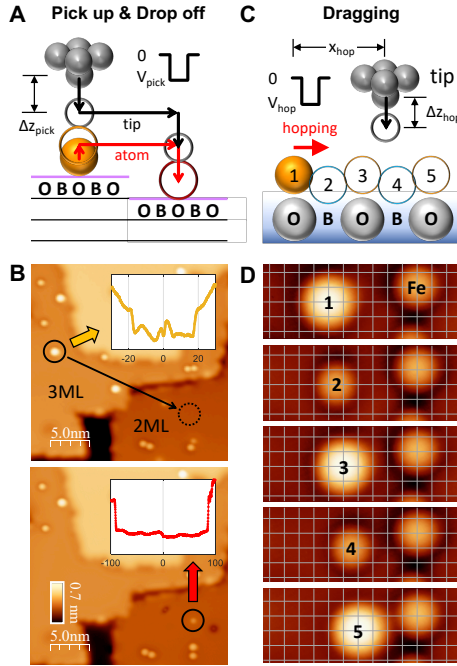


FIG. 3: **Manipulations of Ti atoms on 3ML MgO:** (A) Schematic describing moving a Ti atom by pick-up and subsequent drop-off processes using a STM tip. (B) STM images before (upper) and after (lower) moving a Ti atom from a 3ML to a 2ML MgO patches, respectively, as depicted by the black arrow. The insets are the STS spectra measured before and after moving the atom. (C) Schematic describing hopping of a Ti atom on 3ML MgO using a DC bias voltage pulse. (D) 5 STM images sequentially measured before (1) and after each hopping of a Ti atom from positions 1 to 5, as described in C. The STM images in B and D are measured at $V_b = 100$ mV and $I_{\text{tun}} = 10$ pA.

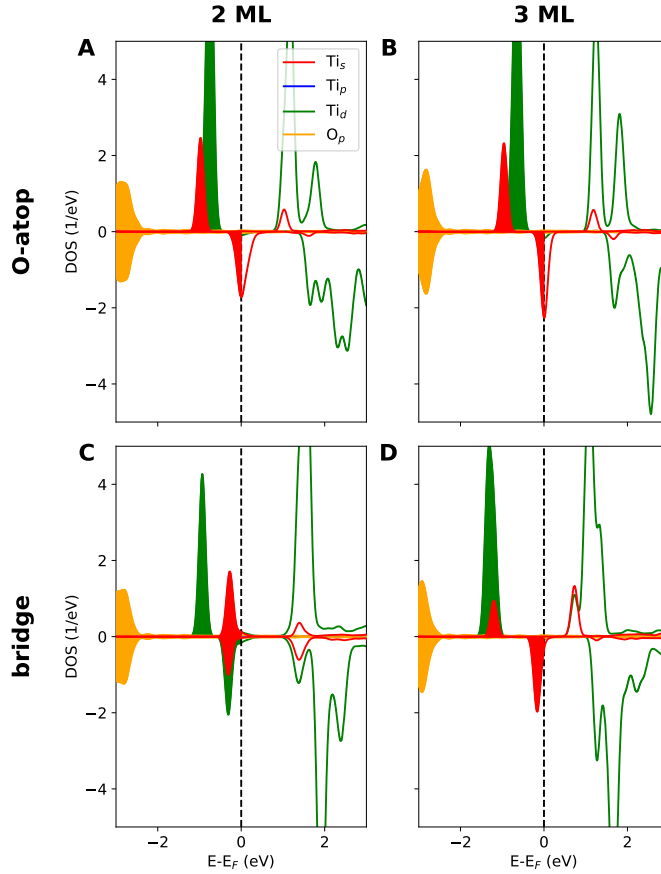


FIG. 4: **PDOS of Ti on MgO/Ag (100).** The density of states projected on s, p, d orbitals of the Ti atom and the nearest oxygen for four cases that have been displayed in columns depending on the number of monolayers (2 ML, 3 ML) of MgO and in rows for the oxygen-atop and bridge sites: (A) $\text{Ti}_O(2)$, (B) $\text{Ti}_O(3)$, (C) $\text{Ti}_B(2)$, (D) $\text{Ti}_B(3)$.

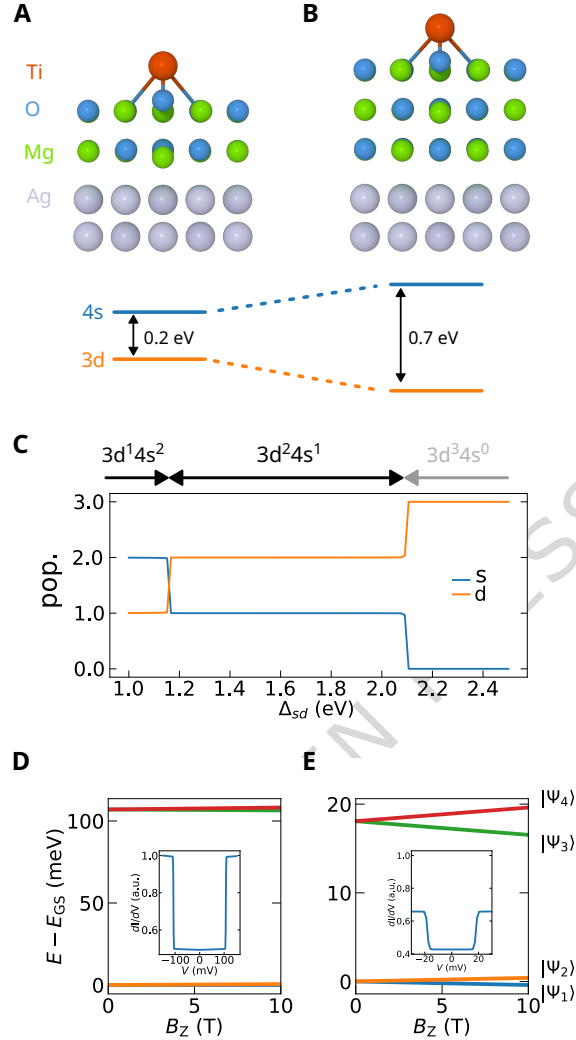
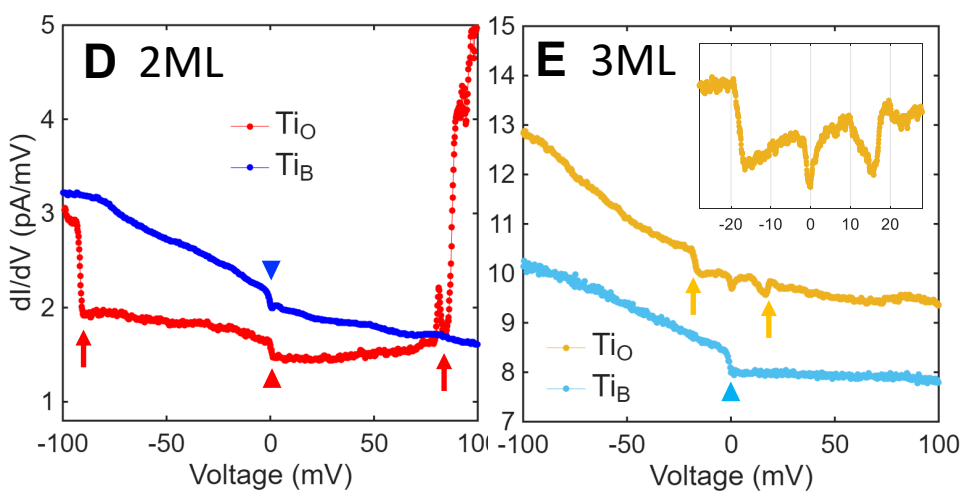
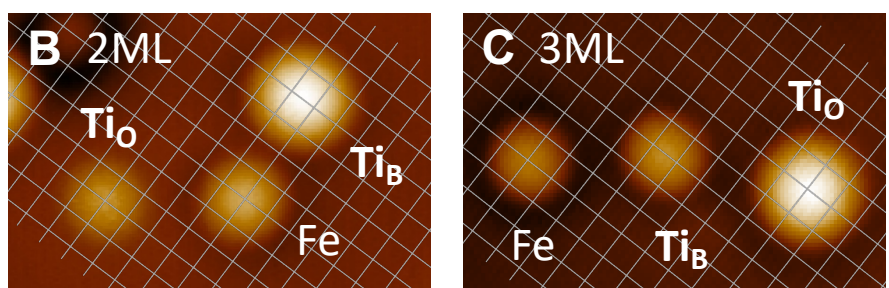
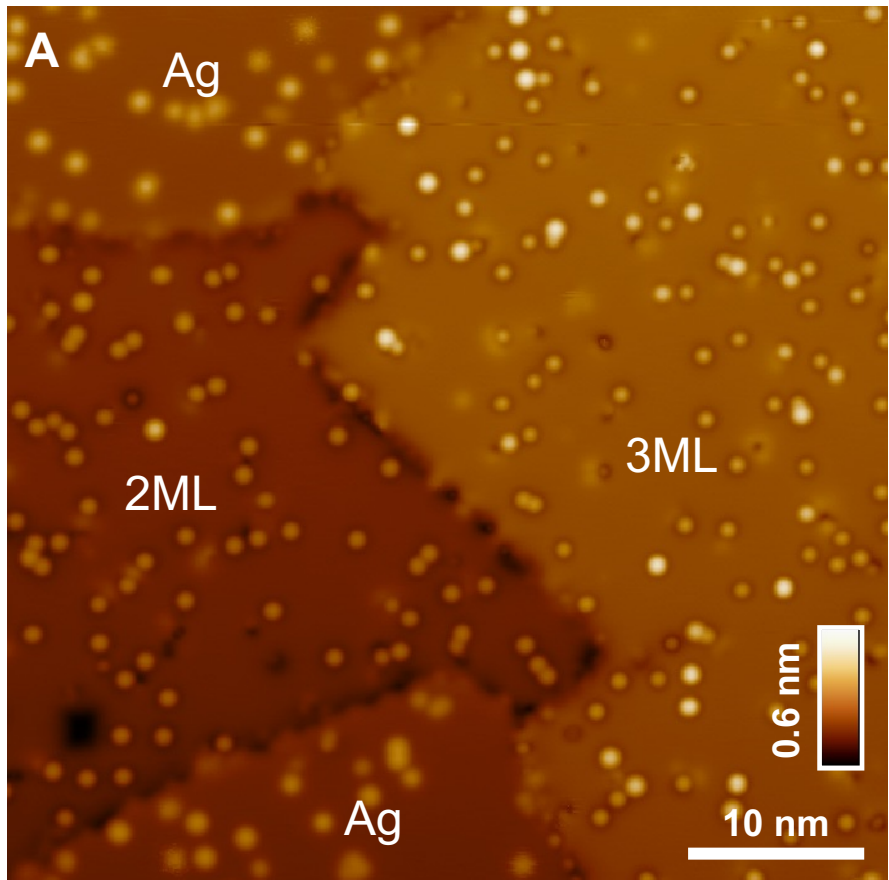
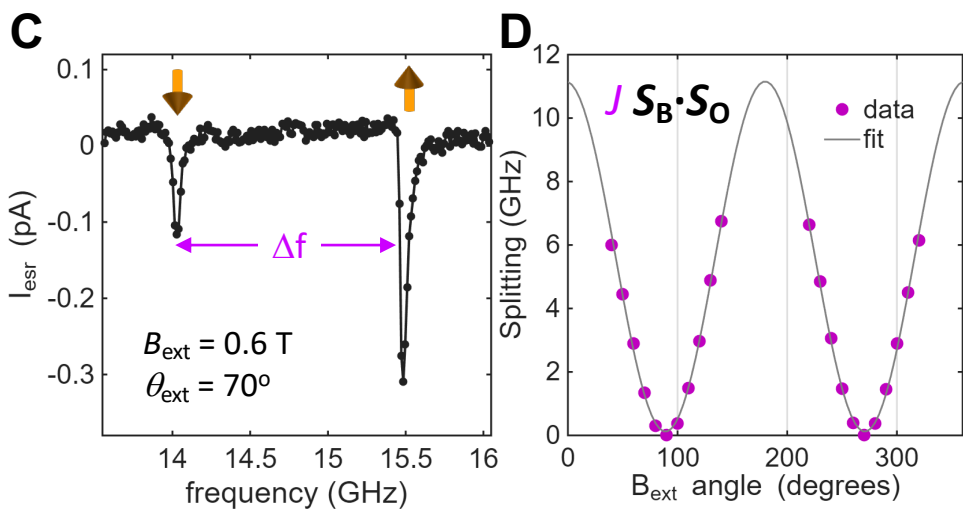
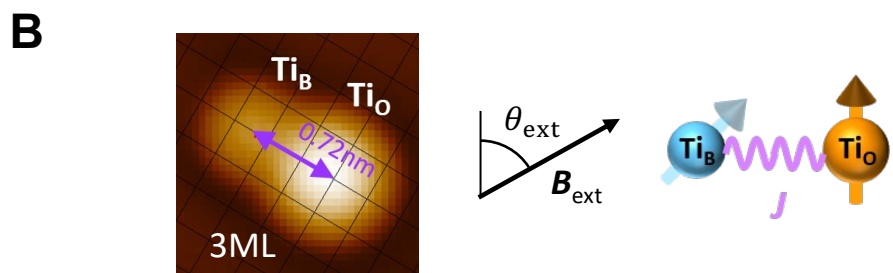
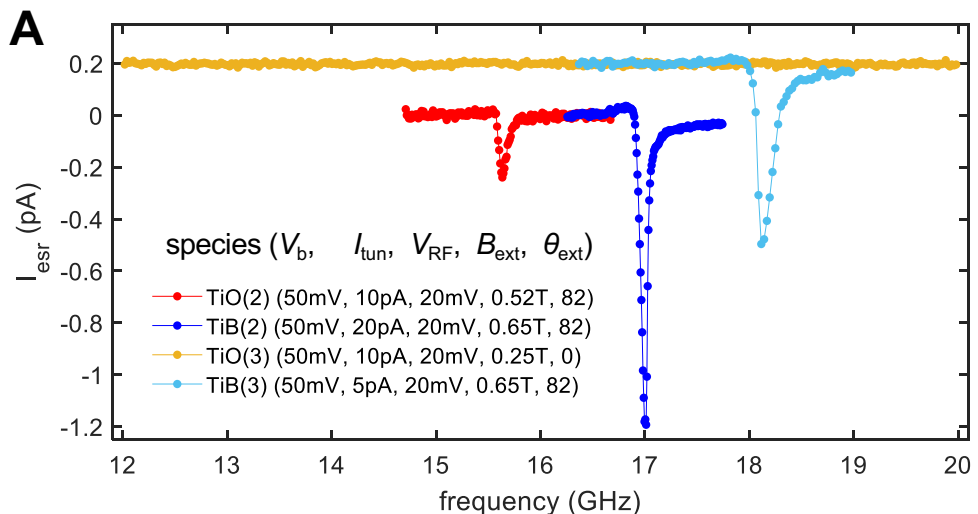
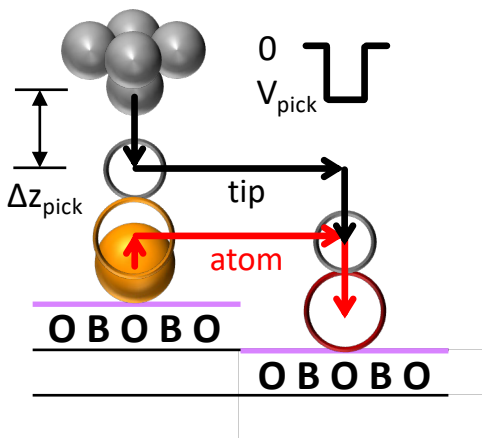
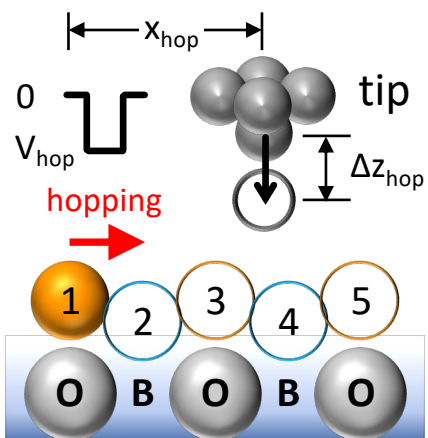
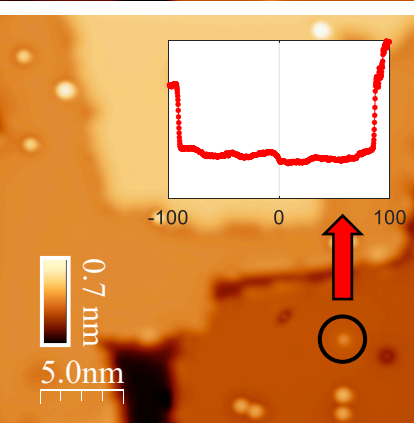
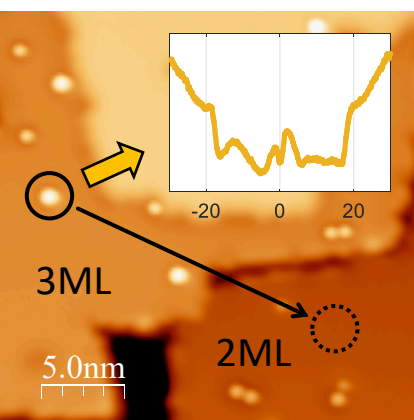
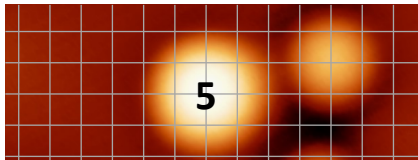
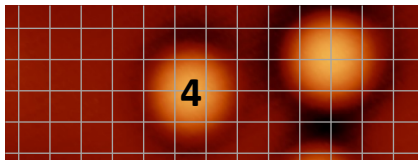
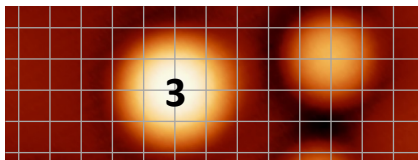
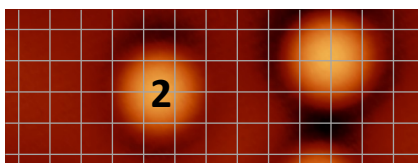
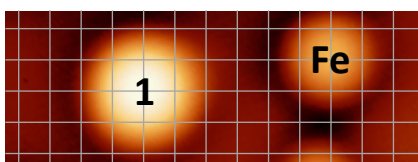
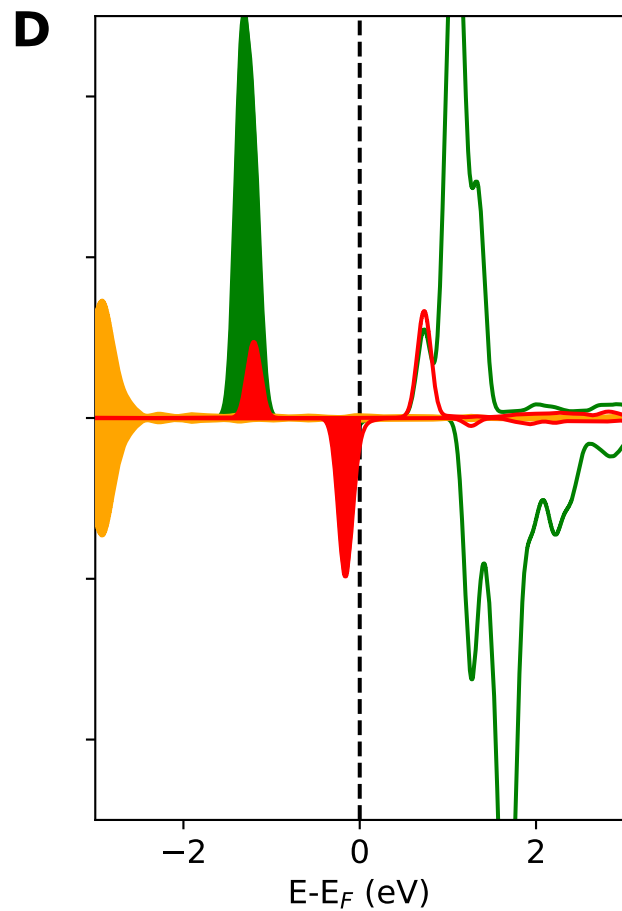
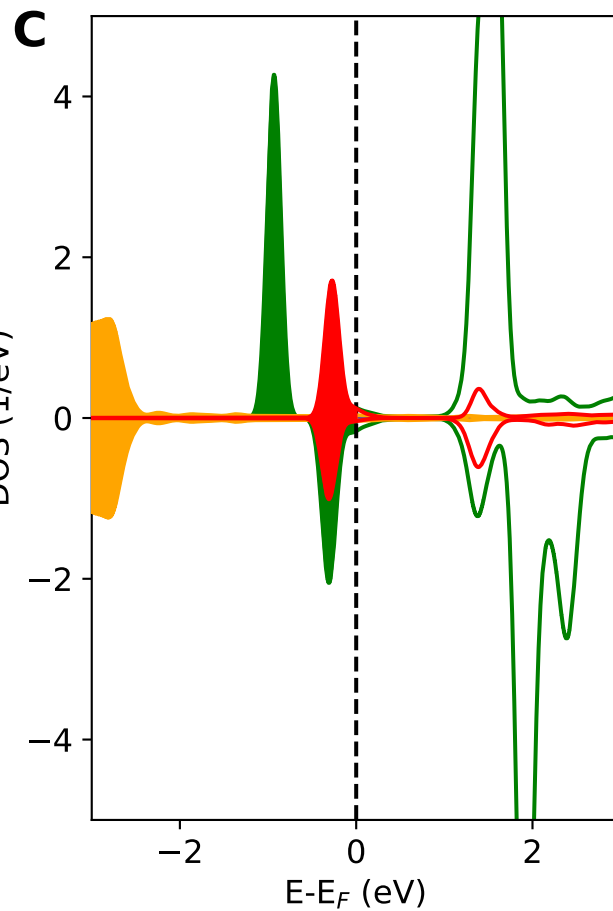
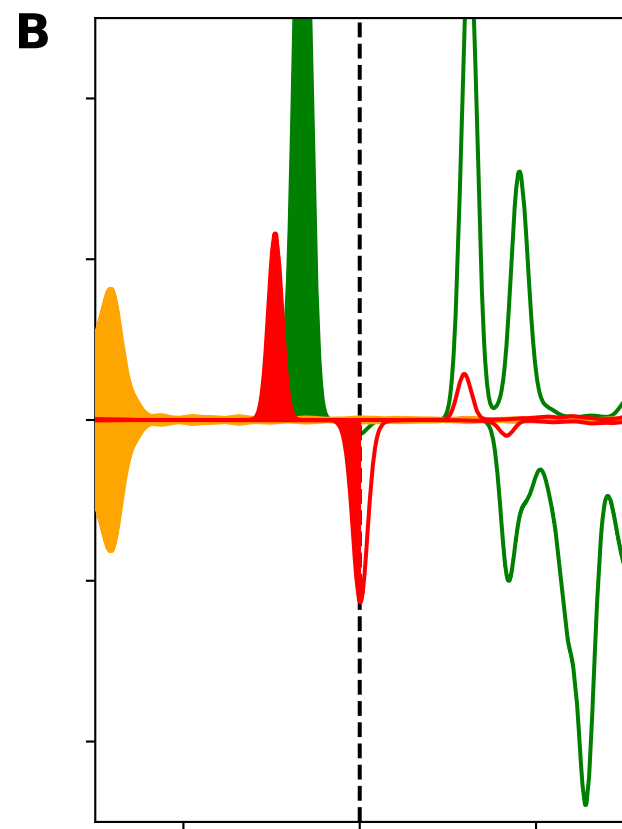
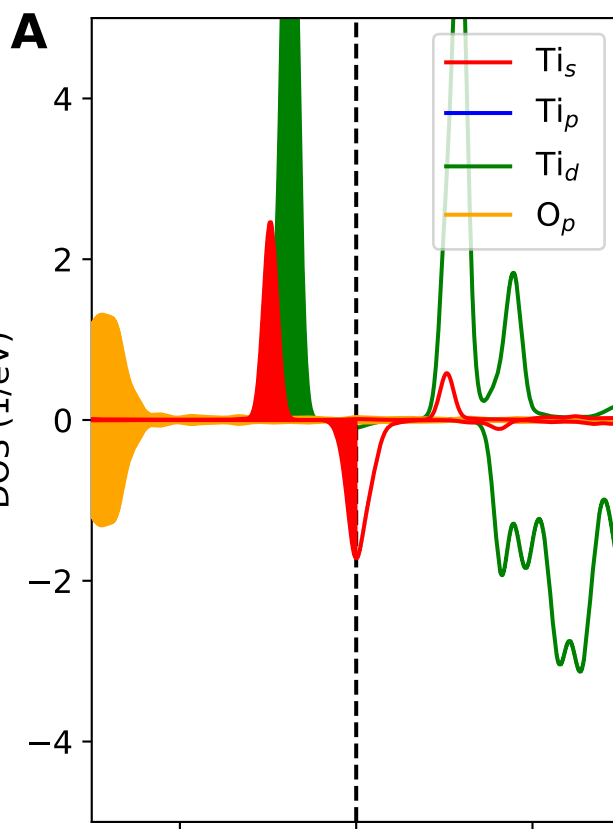


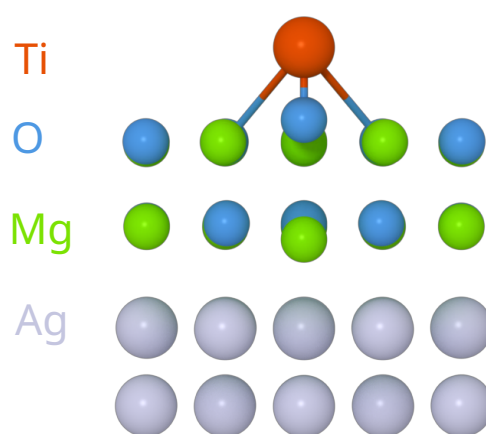
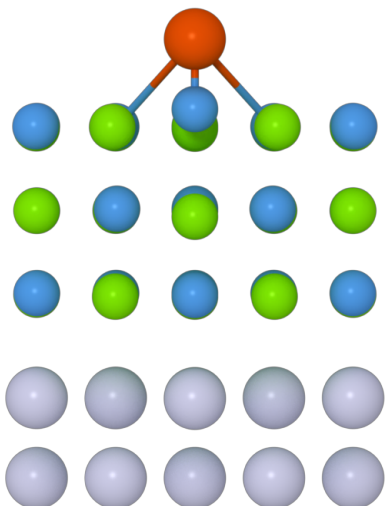
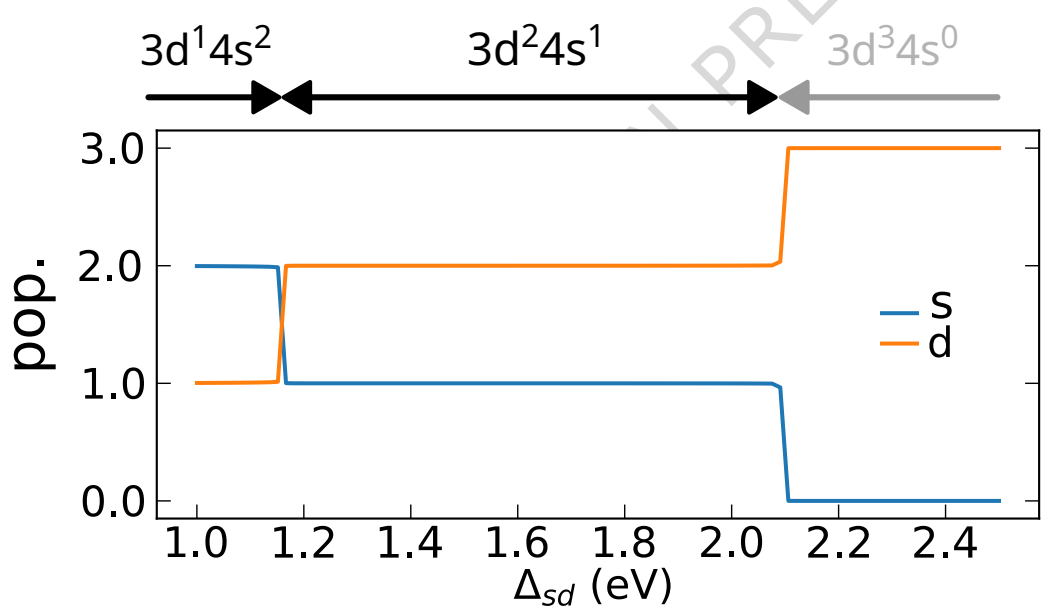
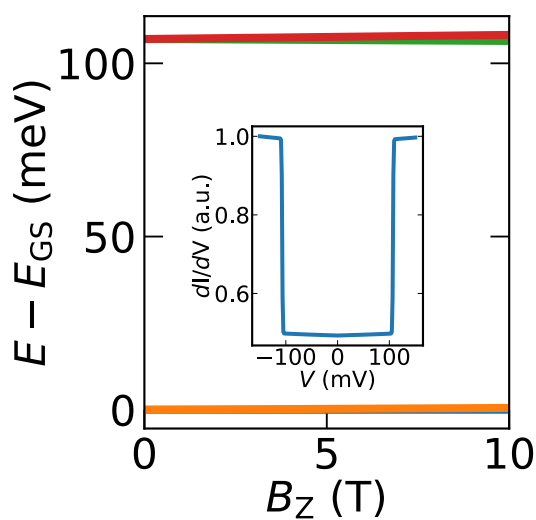
FIG. 5: **Multiplet calculations Ti on $\text{MgO}^{(2)}$ and $\text{MgO}^{(3)}$ on Ag (100).** (A) and (B) show the relaxed geometry of Ti on $\text{MgO}^{(2)}$ and $\text{MgO}^{(3)}$. When going from 2 to 3 ML of MgO the $s - d$ splitting Δ_{sd} increases, as shown schematically below. (C) spin states of the Ti^+ as function of Δ_{sd} . Indicated are three possible orbital configurations for the same charge state. (D) multiplet calculations and simulated dI/dV spectrum (inset) for the case of $3d^1$, showing two strong excitations around 100 meV. The multiplet wave-functions $|\Psi_i\rangle = |S_z, L_z\rangle$ for the first four states in order of increasing energy are $|\Psi_1\rangle = |-0.5, +0.5\rangle$, $|\Psi_2\rangle = |+0.5, -0.6\rangle$, $|\Psi_3\rangle = |-0.5, -0.6\rangle$, $|\Psi_4\rangle = |+0.5, +0.6\rangle$ (E) shows the same calculation for a $3d^2$ orbital configuration, which shows excitations close to 20 meV, in reasonable agreement with the experiment (see inset in Fig. 3B). Here, $|\Psi_1\rangle = |-1, +2.7\rangle$, $|\Psi_2\rangle = |+1, -2.7\rangle$, $|\Psi_3\rangle = |+0.0, -2.7\rangle$, $|\Psi_4\rangle = |-0.0, +2.7\rangle$





A Pick up & Drop off**C Dragging****B****D**

2 ML**3 ML****O-atop****bridge**

A**B****C****D****E**